

# The Self-Consistent Field Study of the Adsorption of Flexible Polyelectrolytes onto Two Charged Nano-objects

Chaohui Tong\* and Yuejin Zhu

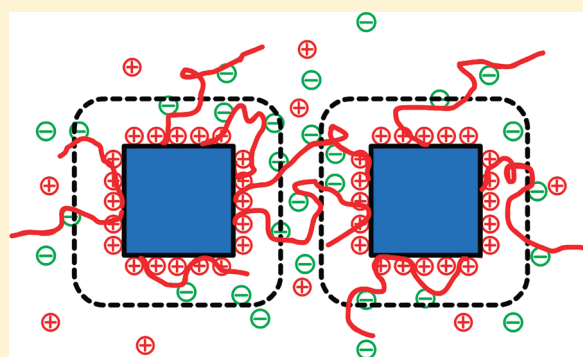
Department of Physics, Ningbo University, Ningbo, 315211, China

The Key Laboratory of Molecular Engineering of Polymers, Ministry of Education of China, Fudan University, Shanghai, 200433, China

Hongdong Zhang, Feng Qiu, Ping Tang, and Yuliang Yang

Department of Macromolecular Science, Fudan University and the Key Laboratory of Molecular Engineering of Polymers, Ministry of Education of China, Shanghai, 200433, China

**ABSTRACT:** The continuum self-consistent field theory (SCFT) is applied to the study of the adsorption of flexible polyelectrolyte (PE) onto the surfaces of two two-dimensional charged square objects with a constant electric field strength immersed in a weakly charged polyelectrolyte solution. The dependences of the different chain conformations, that is, bridging, loop, tail, and train, and in particular, the bridging chain conformation, on various system parameters (the charge fraction of the PE chains, the surface charge density, the object size, the salt concentration, etc.) are investigated. The efficient multigrid method is adopted to numerically solve the modified diffusion equation and the Poisson equation. It is found that the thickness  $L_B$  of the boundary layer of the adsorbed PE chains is independent of the chain length and scales with the surface charge density  $\sigma$  and the fraction of charges on PE chains  $\alpha_P$  as  $L_B \sim \sigma^{-0.36}$  and  $L_B \sim \alpha_P^{-0.36}$ , respectively. Simulation results reveal that the total amount of bridging chain conformation in the system scales linearly with respect to the size of the charge objects and scales linearly with the chain length in the long polymer chain regime. Simulation results reveal that the total amount of the bridging chain conformation in the system scales with the charge fraction of PE chains as a power law and the scaling exponent is dependent on all of the other system parameters. Simulation results show that the total amount of charges on the adsorbed chains in the system can overcompensate the surface charges for relatively long chains with high charge fractions.



## I. INTRODUCTION

The adsorption of polyelectrolytes (PE) on oppositely charged surfaces is an interesting and important problem because of its rich and fascinating physics involved and numerous practical applications.<sup>1–11</sup> PE adsorption is directly related to the colloidal stability and finds many applications in industries such as water treatment, paint making, food processing, and so forth. PE adsorption also has profound implications in biological systems. Many biomolecules, for instance, DNA, are PEs, which can be adsorbed onto the surfaces of oppositely charged proteins and membranes or act as substrates for the adsorption of other PEs.

Although much progress has been made in the theoretical study of PE adsorption on charged surfaces, a complete and transparent physical picture of PE adsorption is still lacking. In such systems, the interactions involved are multiscale in nature, for example, long-range Coulomb interactions and short-range interactions such as van der Waals force between monomers and solvent molecules. Due to the Coulomb interaction and the connectivity of finite-sized monomers bearing charged groups

within long polymer chains, there are quite a few different length scales involved in these systems, for example, the monomer size, the size of electrostatic blobs for relatively long and highly charged polymer chains, the Bjerrum length, the Debye screening length, and so forth. Incorporating the drastically different interactions and length scales into a single theory poses considerable challenges to theorists. Furthermore, in such systems, there are many interplaying physical parameters affecting the adsorption behaviors of PE on charged surfaces. These parameters include those characterizing the PEs, such as the degree of polymerization and the charge distribution along the PE chains, as well as those for solvent molecules, charged surfaces, and added salt ions.

The adsorption of PEs on the surface of a single object with opposite charges has drawn considerable analytical, simulational, and experimental attention.<sup>2–18</sup> The main focus of such studies is

**Received:** May 26, 2011

**Revised:** September 1, 2011

**Published:** September 02, 2011

on the adsorption-depletion behavior and the associated scaling law in terms of the system parameters, as well as the curvature effect of the adsorbing surface on the adsorption-depletion phase-transition-like behavior.<sup>12–18</sup> The adsorption of oppositely charged PEs on the surfaces of two objects (infinite-sized or finite-sized) with the same sign of charges immersed in a polyelectrolyte solution has also attracted intense theoretical, simulation, and experimental research interest.<sup>19–36</sup> Under suitable conditions, one single PE chain can be adsorbed onto the surfaces of two (or more) charged objects, thus acts as a bridge between these two objects, and mediates attractive interactions between them. The “bridging” interaction exactly corresponds to the aforementioned scenario and is crucial to the colloidal stability. Up to now, the central aspect of the research effort is about the effects of various system parameters on the strength and range of the attractive interactions between two objects mediated by bridging PEs. However, there are very few research investigations of the PE chain conformations in the gap between two charged objects. So far, most of the studies of the chain conformations in the vicinity of adsorbing surfaces are limited to the cases of neutral polymer and surfaces. Scheutjens and Fleer developed a lattice model to study the adsorption of neutral polymer chains on single and double flat surfaces.<sup>37–39</sup> The statistical distribution of tails, loops, and bridges can be easily enumerated. For the case of the adsorption of polymer chains on two parallel surfaces, with the decrease of surface separation, there is an increase in the bridging fraction of polymer chains adsorbing on both surfaces simultaneously. Therefore, the study of PE chain conformations in the gap between two charged objects is very interesting and important in elucidating the mechanism governing PEs adsorption behaviors and the bridging effect on colloidal stability, which is the main focus of the present study.

The adsorption of weakly charged and flexible PEs onto the surfaces of two charged objects and the associated chain conformations can be well-described at a quantitative level by the self-consistent field theory (SCFT). Starting from the lattice SCFT for neutral polymer adsorptions developed by Scheutjens and Fleer,<sup>37–39</sup> Van der Schee and Lyklema extended it to the study of the adsorption of PEs.<sup>40</sup> Shi and Wang have independently developed the continuum SCFT of multicomponent weakly charged polyelectrolyte systems.<sup>41,42</sup> In their SCFT, the electrostatic interaction between charges is introduced to the SCFT for neutral polymeric systems through a position-dependent electric potential field, which can be solved by a Poisson–Boltzmann like equation. This SCFT has been successfully applied to the studies of the adsorption of flexible PEs onto surfaces of a flat plane and a charged cylinder, the phase separation of neutral/charged mixed polymer brushes, and the phase behaviors of polyelectrolyte block copolymers.<sup>43–47</sup>

In this work, we have applied the continuum SCFT for PEs to the study of the adsorption of flexible PEs on the surfaces of two two-dimensional charged square objects with a constant electric field strength immersed in a weakly charged polyelectrolyte solution. The main focus is on the dependences of the fractions of tail, loop, and bridge conformations on different controlling parameters, such as the chain length and the charge fraction of PE chains, the surface charge density and the size of the objects, and the separation between the two objects, and so forth. One elegant feature of the continuum SCFT is the rich statistical information contained in the propagator describing the polymer chain segment distribution. Through the analysis of the propagator,

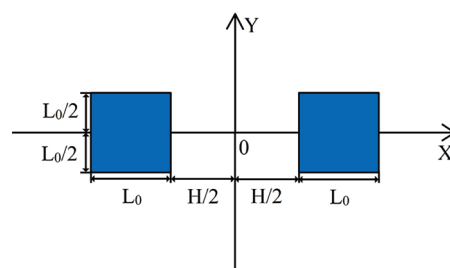


**Figure 1.** A schematic representation of the system under study. The two charged square objects are immersed in a polyelectrolyte solution.

which is solved by a modified diffusion equation in the SCFT, the fractions and spatial distributions of the different chain conformations, that is, loop, tail, and bridge, can be relatively easily obtained. In numerically solving the modified diffusion equation and the Poisson equation, the highly efficient multigrid method is adopted. The rest of the paper is organized as follows. In Section II, the theory and methods used in the present paper are described. In Section III, results and discussions concerning the chain conformations in the system and the degree of charge compensation are presented. In Section IV, the main conclusions are summarized, and the future direction of the present study is presented.

## II. THEORY, MODEL EQUATIONS, AND NUMERICAL METHODS

In this paper, we consider a system of volume  $V$  consisting of two two-dimensional square like-charged objects with a constant surface electric field strength immersed in an oppositely charged polymer solution with mobile point-like monovalent cations and anions and solvent  $S$ . The size of the square objects is denoted as  $L_0$ , and the surface electric field strength is assumed to be equal to that of a sphere with a surface charge density of  $\sigma$  in unit of the elementary charge  $e$  per unit surface area. The two objects are symmetric with respect to the  $y$ -axis, and each object is symmetric with respect to the  $x$ -axis of the system. The width of the gap between the two objects is labeled as  $H$ . For simplicity, the system is assumed to be translational invariant along the  $z$ -axis. A schematic diagram of the system is shown in Figure 1. In essence, the model in this study mimics the adsorption of polyelectrolytes onto two charged cylinders such as DNA.

The continuum SCFT theory for inhomogeneous multicomponent weakly charged polyelectrolyte systems has been derived in refs 41 and 42. According to ref 42, the dimensionless mean-field SCF equations are as follows

$$\phi_P(\vec{r}) + \phi_S(\vec{r}) - 1 = 0 \quad (1)$$

$$\omega_P(\vec{r}) = \chi_{PS} N \phi_S(\vec{r}) + \eta(\vec{r}) \quad (2)$$

$$\omega_S(\vec{r}) = \chi_{PS} N \phi_P(\vec{r}) + \eta(\vec{r}) \quad (3)$$

$$\omega_{\pm} = N \nu_{\pm} \psi(\vec{r}) \quad (4)$$

$$\phi_P(\vec{r}) = \frac{\bar{\Phi}_P}{Q_P} \int_0^1 ds q(\vec{r}, s) q(\vec{r}, 1-s) \quad (5)$$

$$\phi_M(\vec{r}) = \frac{\bar{\Phi}_M}{Q_M} \exp \left[ -\frac{\omega_M(\vec{r})}{N} \right] \quad (6)$$

$$\vec{\nabla} \cdot [\varepsilon(\vec{r}) \vec{\nabla} \psi(\vec{r})] = -N[\alpha_P \nu_P \phi_P(\vec{r}) + \nu_+ \phi_+(\vec{r}) + \nu_- \phi_-(\vec{r})] \quad (7)$$

where  $\phi_j$  with  $j = P, S$ , and  $\pm$  are the dimensionless volume fractions of PE chains, solvent molecules, and mobile ions,  $\chi_{PS}$  denotes the Flory–Huggins interaction parameter between monomers and solvent molecules,  $\eta(\vec{r})$  is the Lagrange multiplier to enforce the incompressible condition,  $\omega_j$  denotes the conjugate interaction field within the SCFT formalism,  $\psi(\vec{r})$  denotes the electric potential field, the volume-averaged densities  $\bar{\Phi}_P \equiv n_P N / (\rho_0 V)$ , and  $\bar{\Phi}_M \equiv n_M / (\rho_0 V)$  with  $n_P$  and  $n_M$  representing respectively the total number of PE chains with chain length  $N$  and species  $M$  ( $M = S, +, -$ ),  $\rho_0$  denotes the same density of PE segments and the solvent molecules,  $\varepsilon(\vec{r})$  denotes the permittivity,  $\alpha_P$  denotes the average degree of ionization of PE chains with the smeared charge distribution,  $\nu_P = -1$  and  $\nu_{\pm} = \pm 1$  are for the charge valences of PE chains and the mobile ions, respectively, and  $Q_P = \int d\vec{r} q(\vec{r}, 1) / V$  and  $Q_M = \int d\vec{r} \exp[-\omega_M(\vec{r}) / N] / V$ . In the present study, the permittivity of the medium is assumed to be a constant, the same as that of the pure water. In the above SCF equations, the nondimensionalization is performed in the same way as that in ref 42, except that the permittivity of the medium is rescaled as  $6\varepsilon(\vec{r})k_B T / (\rho_0 e^2 a^2) \rightarrow \varepsilon(\vec{r})$  with  $k_B$  the Boltzmann constant and  $T$  the absolute temperature in this paper instead of  $3\varepsilon(\vec{r})k_B T / (2\pi\rho_0 e^2 a^2) \rightarrow \varepsilon(\vec{r})$  in ref 42. The two ways of nondimensionalization of the permittivity differ by a factor of  $4\pi$ .

The propagator  $q(\vec{r}, s)$  corresponding to the probability of finding the end-segment of a polymer chain of length  $s$  at  $\vec{r}$  satisfies the following modified diffusion equation

$$\frac{\partial q(\vec{r}, s)}{\partial s} = \nabla^2 q(\vec{r}, s) - [\omega_P(\vec{r}) + N\alpha_P \nu_P \psi(\vec{r})] q(\vec{r}, s) \quad (8)$$

with the initial condition  $q(\vec{r}, 0) = 1$  outside the solid charged objects and the boundary condition  $q(\vec{r}, s) = 0$  on the surfaces of the objects. The mean-field free energy per chain is

$$f = \frac{1}{V} \int d\vec{r} \left[ \chi_{PS} N \phi_P \phi_S - \omega_P \phi_P - \omega_S \phi_S - \frac{\varepsilon}{2} |\vec{\nabla} \psi|^2 \right] - N \left[ \frac{\bar{\Phi}_P}{N} \ln \left( \frac{Q_P}{\bar{\Phi}_P} \right) + \bar{\Phi}_S \ln \left( \frac{Q_S}{\bar{\Phi}_S} \right) + \bar{\Phi}_+ \ln \left( \frac{Q_+}{\bar{\Phi}_+} \right) + \bar{\Phi}_- \ln \left( \frac{Q_-}{\bar{\Phi}_-} \right) \right] \quad (9)$$

The Poisson equation (eq 7) is numerically solved by the standard multigrid method.<sup>48,49</sup> To deal with the Neumann type boundary condition on the surfaces of the two charged objects, the domain decomposition method is employed with the solid objects excluded from the computational domain.<sup>50</sup>

The modified diffusion equation (eq 8) is also numerically solved by the multigrid method. The right-hand side of the equation is discretized using the Crank–Nicolson method, as shown by the following

$$\frac{q_{i,j}^{n+1} - q_{i,j}^n}{\Delta s} = \frac{1}{2} [\nabla^2 q_{i,j}^{n+1} - \omega_{i,j}^n q_{i,j}^{n+1}] + \frac{1}{2} [\nabla^2 q_{i,j}^n - \omega_{i,j}^n q_{i,j}^n] \quad (10)$$

After a rearrangement of eq 10, a Poisson-type equation is obtained

$$\left[ \frac{1}{\Delta s} - \frac{1}{2} \nabla^2 + \frac{1}{2} \omega_{i,j}^n \right] q_{i,j}^{n+1} = \left[ \frac{1}{\Delta s} + \frac{1}{2} \nabla^2 - \frac{1}{2} \omega_{i,j}^n \right] q_{i,j}^n \quad (11)$$

which can be efficiently solved by the multigrid method. To apply the Dirichlet boundary condition for the propagator on the surfaces of the two charged objects, the domain decomposition method is also adopted.

To calculate the structure and conformation of the adsorbed polymer chains, the region between the surface of each object and the second inflection point of the polymer density profile away from the object is defined as the boundary layer of the corresponding object.<sup>18</sup> The rest of the domain exterior to the two boundary layers is denoted as the adsorbed layer. To examine the different conformations of polymer chains in the adsorbed layer, the propagator corresponding to free chains in the adsorbed layer with none of their segments falling into the two boundary layers, which is denoted as  $q^f(\vec{r}, s)$ , is obtained first. The propagators corresponding to the adsorbed chains with any of their segments in either of the two boundary layers, which are denoted as  $q_I^a(\vec{r}, s)$  and  $q_{II}^a(\vec{r}, s)$  (the subscripts I and II denote the boundary layer of the left and right object), respectively, are obtained next by using the following relationships

$$q_I^a(\vec{r}, s) = q_I(\vec{r}, s) - q^f(\vec{r}, s) \quad (12)$$

$$q_{II}^a(\vec{r}, s) = q_{II}(\vec{r}, s) - q^f(\vec{r}, s) \quad (13)$$

where  $q_I(\vec{r}, s)$  and  $q_{II}(\vec{r}, s)$  denote the propagators of polymer chains with none of their segments falling into the boundary layers of the right object and left object, respectively.  $q^f(\vec{r}, s)$ ,  $q_I(\vec{r}, s)$ , and  $q_{II}(\vec{r}, s)$  satisfy the same modified diffusion equation as  $q(\vec{r}, s)$ , but with different boundary conditions.  $q^f(\vec{r}, s)$  vanishes on the surfaces of the two boundary layers,  $q_I(\vec{r}, s)$  vanishes on the surfaces of the left object and the boundary layer of the right object, and  $q_{II}(\vec{r}, s)$  vanishes on the surfaces of the right object and the boundary layer of the left object. Because the modified diffusion equation needs to be solved only once to obtain each of  $q^f(\vec{r}, s)$ ,  $q_I(\vec{r}, s)$ , and  $q_{II}(\vec{r}, s)$ , the forward-time central-space (FTCS) numerical scheme is used for numerical convenience.

Using the propagators of the adsorbed chains and free chains, the volume fractions contributed from the different chain conformations in the adsorbed layer can be obtained:

$$\phi^f(\vec{r}) = \frac{\bar{\Phi}_P}{Q_P} \int_0^1 ds q^f(\vec{r}, s) q^f(\vec{r}, 1-s) \quad (14)$$



$$\phi_I^l(\vec{r}) = \frac{\bar{\Phi}_P}{Q_P} \int_0^1 ds q_I^a(\vec{r}, s) q_I^a(\vec{r}, 1-s) \quad (15)$$

$$\phi_{II}^l(\vec{r}) = \frac{\bar{\Phi}_P}{Q_P} \int_0^1 ds q_{II}^a(\vec{r}, s) q_{II}^a(\vec{r}, 1-s) \quad (16)$$

$$\phi_I^t(\vec{r}) = 2 \frac{\bar{\Phi}_P}{Q_P} \int_0^1 ds q_I^a(\vec{r}, s) q^f(\vec{r}, 1-s) \quad (17)$$

$$\phi_{II}^t(\vec{r}) = 2 \frac{\bar{\Phi}_P}{Q_P} \int_0^1 ds q_{II}^a(\vec{r}, s) q^f(\vec{r}, 1-s) \quad (18)$$

where  $\phi^f(\vec{r})$  denotes the density of free chains with none of their segments in the boundary layers of the two charged objects,  $\phi_I^l(\vec{r})$  and  $\phi_I^t(\vec{r})$  are the loop and tail fractions in the adsorbed layer corresponding to the left object, and  $\phi_{II}^l(\vec{r})$  and  $\phi_{II}^t(\vec{r})$  are the loop and tail fractions corresponding to the right object. Finally, the volume fraction contributed by the bridging conformation can be obtained:

$$\begin{aligned} \phi^b(\vec{r}) &= \phi_P(\vec{r}) - \phi^f(\vec{r}) - \phi_I^l(\vec{r}) \\ &\quad - \phi_I^t(\vec{r}) - \phi_{II}^l(\vec{r}) - \phi_{II}^t(\vec{r}) \end{aligned} \quad (19)$$

Analogously, we can obtain the volume fraction contributed by the bridging conformation inside the boundary layers.  $q_I^t(\vec{r}, s)$  and  $q_{II}^t(\vec{r}, s)$ , which denote the propagators of polymer chains with none of their segments falling outside the boundary layers of the left object and right object, respectively, are obtained first. Next, the propagators corresponding to the adsorbed chains with any of their segments outside either of the two boundary layers, which are denoted as  $q_I^{ab}(\vec{r}, s)$  and  $q_{II}^{ab}(\vec{r}, s)$ , respectively, are obtained, that is,  $q_I^{ab}(\vec{r}, s) = q_I(\vec{r}, s) - q_I^t(\vec{r}, s)$  and  $q_{II}^{ab}(\vec{r}, s) = q_{II}(\vec{r}, s) - q_{II}^t(\vec{r}, s)$ . Using expressions similar to those in eqs 14–18, we can obtain the volume fractions contributed from the different chain conformations (train, tail, and loop conformations for each boundary layer) inside the two boundary layers. For example, the volume fraction of the train conformation inside the boundary layer of the left object is calculated as  $\phi_I^t(\vec{r}) = (\bar{\Phi}_P/Q_P) \int_0^1 ds q_I^t(\vec{r}, s) q_I^t(\vec{r}, 1-s)$ . Finally, the volume fraction contributed by the bridging conformation inside the boundary layers is obtained by subtracting the six terms of volume fractions from  $\phi_P(\vec{r})$ , similar to what is done in eq 19.

To quantify the total amount of the bridging chain conformation due to the adsorption of PE on the two charged objects, we introduce the parameter  $\Sigma = \int_V \phi^b(\vec{r}) d\vec{r}$ , where the subscript “V” denotes the volume of the whole system.

To quantify the total amount of the adsorbed PE chains in the system, we introduce the parameter of the degree of charge compensation  $\Gamma$ , which is defined as the ratio of the total amount of charges on the adsorbed PE chains in the system to the total amount of opposite charges on the surface of the objects, that is,

$$\Gamma = \int_V \alpha_P [\phi_P(\vec{r}) - \phi^f(\vec{r})] d\vec{r} / Q \quad (20)$$

where  $\phi^f(\vec{r})$  is the volume fraction of the free chains in the system (see eq 14), and  $Q$  is the total amount of charges on the surface of the objects. The surface charges are only partially compensated when  $\Gamma < 1$ , exactly compensated when  $\Gamma = 1$ , and overcompensated (charge reversal) when  $\Gamma > 1$ . To quantify the total amount of charges carried by the co-ions in the boundary

layer, the parameter  $\Gamma_c$  is introduced, which is defined as  $\Gamma_c = \int_{BL} \phi_{-}(\vec{r}) d\vec{r} / Q$ , where the subscript “BL” denotes the boundary layer.

In the simulations, the grid size of the computational domain is around  $0.0625R_g$ , and the time step size is 0.01 which corresponds to discretizing the polymer chain spatial thread into 100 equal intervals. For both the Poisson equation and the modified diffusion equation, the periodic boundary condition is used along the periphery of the system.

### III. RESULTS AND DISCUSSION

In this paper, the segment size is fixed as  $a = 0.7$  nm, and the number of segments on one PE chain is chosen as  $N = 10, 20, 35, 50$ , and  $70$ . The Flory–Huggins parameter is  $\chi_{PS} = 0.5$  or  $0.0$ ; the charge fraction of a PE chain is varied from  $\alpha_P = 0.05$  to  $\alpha_P = 0.4$ , and the volume-averaged densities  $\bar{\Phi}_P$  is varied from  $0.01$  to  $0.05$ . The dimensionless dielectric constant of the system is fixed at  $\varepsilon = 0.4762$ , which corresponds to the dielectric constant of the pure water at the room temperature. The size of the charged objects is varied from  $L_o = 2.887a$  to  $L_o = 4 \times 2.887a$ , which corresponds respectively to  $1.0R_g$  and  $4.0R_g$  of a flexible PE chain with  $N = 50$ . In solving the Poisson equation, the Neumann boundary condition on the charged surfaces is  $(\partial\psi/\partial r)|_{BC} = (6N)^{1/2} \sigma a^2 / \varepsilon$  in the dimensionless form. The product of  $\sigma$  and  $a^2$  is varied from  $\sigma a^2 = 0.02381$  to  $\sigma a^2 = 0.19048$ , which corresponds to a charge density of  $\sigma = 4.857 \times 10^{-2} \text{ nm}^{-2}$  to  $\sigma = 3.8856 \times 10^{-1} \text{ nm}^{-2}$ . Because the SCFT theory is only valid on the mean-field level and the PE chains are assumed to be flexible, we have checked the range of applicability of the key parameters, that is, the averaged degree of ionization  $\alpha_P$  and the surface charge density  $\sigma$ . The range of  $\alpha_P$  can be estimated by equating the electrostatic energy of a charged polymer coil in a  $\theta$  solvent to the thermal energy

$$\frac{(N\alpha_P)^2 e^2}{\varepsilon_r \varepsilon_0 (N^{1/2} a)} \sim k_B T \Rightarrow \alpha_P \sim N^{-3/4} a^{1/2} l_B^{-1/2} \quad (21)$$

where  $\varepsilon_0$  denotes the vacuum permeability,  $\varepsilon_r$  is the dielectric constant of the water solvent, and  $l_B = e^2 / (\varepsilon_r \varepsilon_0 k_B T)$  is the Bjerrum length which is about  $7.0 \times 10^{-10} \text{ m}$  in water at the room temperature. For a chain length  $N = 50$ ,  $\alpha_P \sim 0.05$ . Thus,  $\alpha_P \in [0.05–0.4]$  used in this paper is not far away from this estimate. The range of the surface charge density can be estimated from the electrostatic coupling parameter  $\Xi$  proposed by Netz et al.<sup>10</sup>

$$\Xi = \frac{l_B}{\mu} = 4\pi l_B^2 \sigma \quad (22)$$

where  $\mu = 1 / (4\pi l_B \sigma)$  denotes the Gouy–Chapman length. For the mean-field theories to be applicable,  $\Xi \leq 1$ . For  $\sigma a^2 = 0.04762$  used in this paper,  $\Xi \approx 0.6$ . Thus, the surface charge densities used in this paper are reasonable from the mean-field point of view.

**1. Interactions between the Two Charged Objects.** As pointed out in the Introduction section, there is considerable theoretical, computational, and experimental evidence that oppositely charged polyelectrolyte chains bridging two like-charged objects immersed in a polyelectrolyte solution can confer an attractive interaction on the two charged objects. In this paper, it would be of interest to study the interaction between such two charged objects using the SCFT.

The free energy  $f$  per chain contains the enthalpic and entropic contributions, that is,  $f = U - TS$ . It can be split into various

**Table 1. Various Enthalpic and Entropic Contributions to the Free Energy per Chain of a Polyelectrolyte Salt-Free Solution with Immersed Two Charged Objects at Different Gap Spacings<sup>a</sup>**

	$H = 6.0R_g$	$H = 5.20R_g$	$H = 4.50R_g$	$H = 3.80R_g$
$U_\chi/k_B T$	0.24738	0.24735	0.24726	0.24712
$U_e/k_B T$	-0.02966	-0.02964	-0.02963	-0.02968
$S_p/k_B$	0.04939	0.05063	0.05164	0.05261
$S_s/k_B$	0.49729	0.49726	0.49717	0.49703
$S_+/k_B$	0.18471	0.18359	0.18285	0.18231
$S_-/k_B$	0.47170	0.47503	0.47769	0.48020
$f/k_B T$	-0.98538	-0.98880	-0.99172	-0.99470

<sup>a</sup> The system parameters are:  $N = 50$ ,  $\chi_{PS} = 0.5$ ,  $\bar{\phi}_p = 0.01$ ,  $\alpha_p = 0.05$ ,  $\sigma a^2 = 0.04762$ ,  $L_o = 2.887a$  which corresponds exactly to the radius of gyration of the PE chains with  $N = 50$ , and the system size of  $(14.0 \times 2.887a) \times (7.0 \times 2.887a)$ . There is no added salt in the system. In solving the self-consistent field equations, the size of the time step is 0.002, and the mesh size is  $0.03125R_g$ .

enthalpic and entropic terms:  $U = U_\chi + U_e$  and  $S = S_p + S_s + S_+ + S_-$ , with each term having the following expression:  $U_\chi/k_B T = \int d\vec{r} \chi_{PS} N \phi_p \phi_s / V$ ,  $U_e/k_B T = \int d\vec{r} [-\epsilon |\vec{\nabla} \psi|^2 / 2] / V$ ,  $S_p/k_B = \bar{\phi}_p \ln(Q_p / \bar{\phi}_p) + \int d\vec{r} \omega_p \phi_p / V$ ,  $S_s/k_B = N \bar{\phi}_s \ln(Q_s / \bar{\phi}_s) + \int d\vec{r} \omega_s \phi_s / V$ ,  $S_+/k_B = N \bar{\phi}_+ \ln(Q_+ / \bar{\phi}_+)$ , and  $S_-/k_B = N \bar{\phi}_- \ln(Q_- / \bar{\phi}_-)$ .

In the systems studied, the number density of the particles is chosen quite high to maximize the bridging effect. A manifesting example of the emergence of an attractive interaction between the two charged objects is shown in Table 1. It can be seen from Table 1 that the relative energy change at different particle separations is on the order of  $10^{-3}$ , and the overall relative energy change between the largest and the smallest particle separation is about 1%. Furthermore, as revealed by the data shown in Table 1, the impact of the bridging effect of PE chains between the two charged objects on the free energy of one polyelectrolyte chain stems from the entropic effects of polymer chains, counterions, and co-ions, that is,  $S_p/k_B$ ,  $S_+/k_B$ , and  $S_-/k_B$ . However, when system parameters corresponding to Table 1 are changed to  $\alpha_p = 0.2$ ,  $\sigma = 0.09524$ ,  $\bar{\phi}_p = 0.02$ , the relative energy change at different particle separations drops to the order of  $10^{-4} \sim 10^{-5}$ . This drop is presumably due to the overwhelming entropic effects of polymer chains, counterions, and co-ions over the bridging effect. Because the primary focus of this paper is on the dependences of the fractions of tail, loop, train, and bridging conformations, as well as the charge compensation parameter upon the system parameters, how the interaction between the two charged objects are affected by the system parameters will not be further discussed.

**2. Dependence of the Different Chain Conformations on the Separation between the Two Charged Objects and the Chain Length.** **2.1. Dependence of the Different Chain Conformations on the Separation between the Two Charged Objects.** Using the PE density profiles, we have calculated the thickness of the boundary layer of the adsorbed PE chains at different system parameters at a large enough object separation which corresponds to the scenario of two independent charged objects immersed in a PE solution. It is found that the thickness of the boundary layer is on the order of the size of the polymer chain, dependent on the surface charge density  $\sigma$ , the fraction of charge on the PE chains  $\alpha_p$ , and the salt concentration. These dependences will be examined in subsequent sections. An important

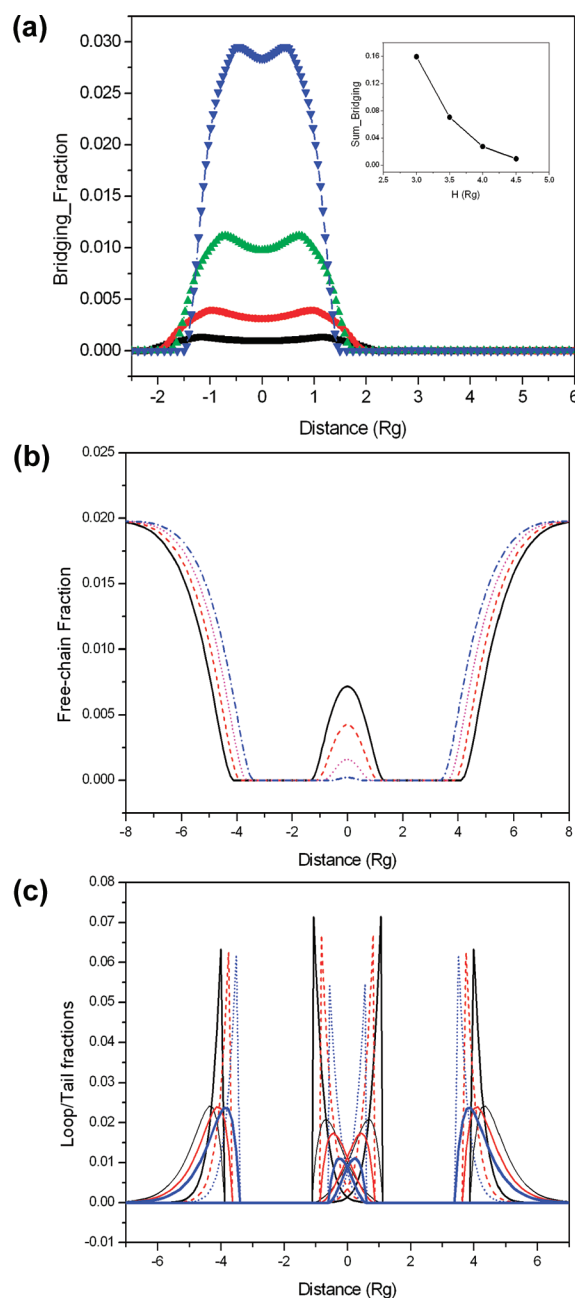


**Figure 2.** (a) Density distribution of the bridging chains along the central horizontal line ( $x$ -axis) for a specified system parameters of  $N = 50$ ,  $\chi_{PS} = 0.5$ ,  $\bar{\phi}_p = 0.02$ ,  $\alpha_p = 0.2$ ,  $\sigma a^2 = 0.09524$ ,  $L_o = 2.887a$  ( $1.0R_g$  for polyelectrolyte chains with  $N = 50$ ), and the system size of  $(74.0 \times 2.887a) \times (73.0 \times 2.887a)$ . There is no added salt in the system. In the inset, the total amount of the bridging chain fraction  $\Sigma$  is displayed. In the figure, the curves with increasing heights correspond respectively to a gap spacing of  $4.50R_g$ ,  $4.0R_g$ ,  $3.50R_g$ , and  $3.00R_g$ . (b) The density distribution of the free chains along the central horizontal line ( $x$ -axis) for the same system as in part a. The labels for the different plots are the same as those in part a. (c) The three sets of plots with sharp peaks with height about 0.06 correspond to the density distributions of the loop conformation along the central horizontal line ( $x$ -axis) for the same system as in part a with a gap spacing of  $4.0R_g$  (solid line),  $3.50R_g$  (dashed line), and  $3.00R_g$  (dotted line). The other three sets of plots are the density distributions of the tail conformation along the central horizontal line ( $x$ -axis) for the same system as in part a with a gap spacing of  $4.0R_g$  (thin solid line),  $3.50R_g$  (solid line), and  $3.00R_g$  (thick solid line). Please note that only the density distributions of the loop and tail conformations in the adsorption layer are shown.

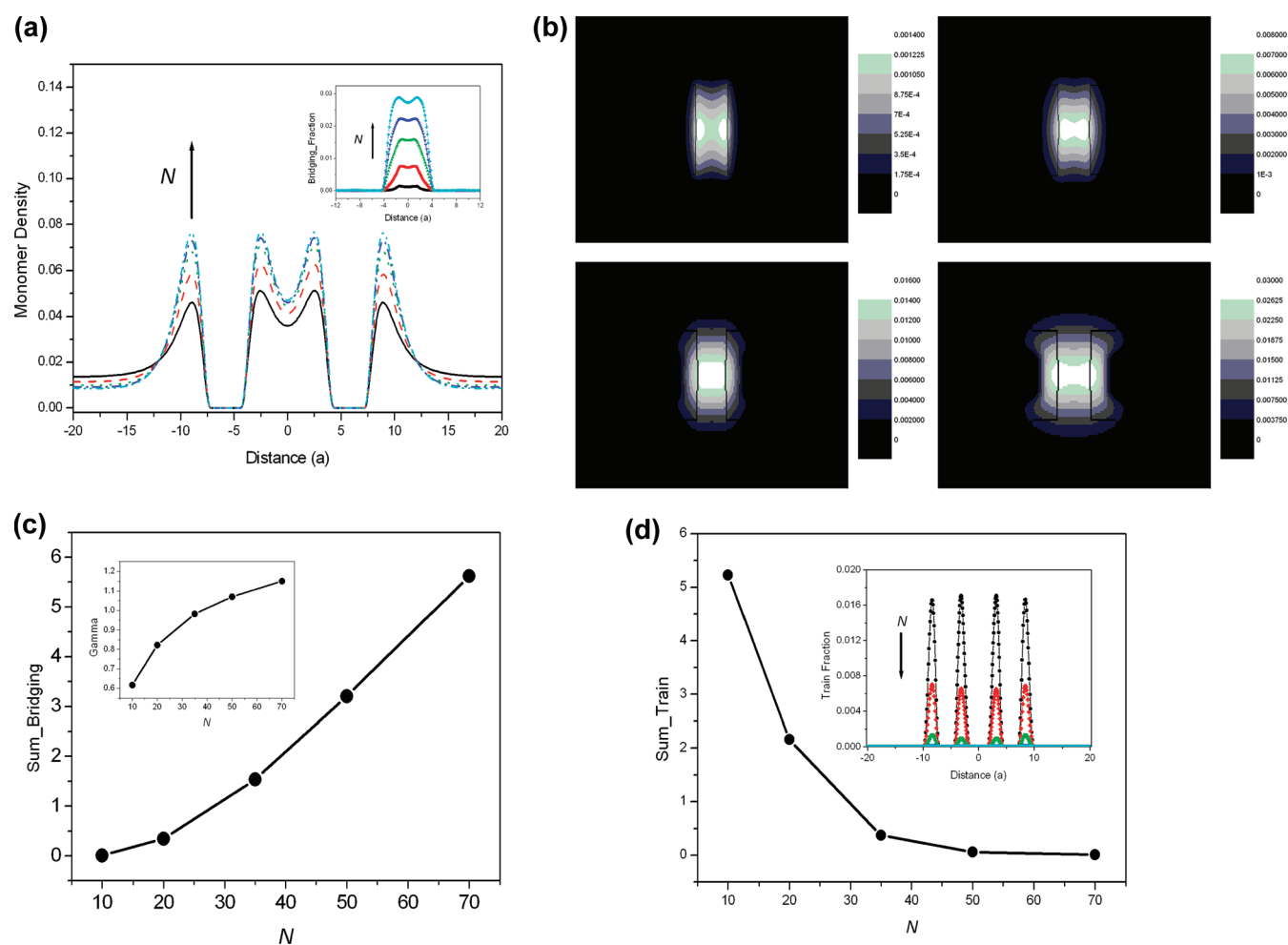


**Figure 3.** (a) Polymer density profiles along the  $x$ -axis at a set of system parameters of  $\chi_{PS} = 0.5$ ,  $\bar{\phi}_P = 0.02$ ,  $\alpha_P = 0.2$ ,  $\sigma a^2 = 0.09524$ ,  $L_o = 2.887a$ ,  $H = 3.0 \times 2.887a$ , and the system size of  $(14.0 \times 2.887a) \times (7.0 \times 2.887a)$  for PE chains with different chain lengths. There is no added salt in the system. In the inset, the density distributions for the bridging chain conformation along the  $x$ -axis at different chain lengths are displayed. In the figure, the profiles with increasing peak values correspond respectively to PE chain lengths of 10, 20, 35, 50, and 70. Note that the  $x$ -axis is in unit of monomer size  $a$ . (b) The contour plots of the volume fractions of the bridging chain conformation for the same systems as in part a. The plots from the left to the right columns and the top to the bottom rows correspond respectively to  $N = 10, 20, 35$ , and  $70$ . Please note the different scales in the scale bars in each plot. Please note that the dark curves correspond to the interface between the boundary layer and the adsorption layer. (c) The plot of the total amount of the bridging chain conformation  $\Sigma$  against the chain length for the same systems as in part a. The  $y$ -axis is in unit of  $a^2/6$ . In the inset, the degree of charge compensation  $\Gamma$  is plotted against the chain length. (d) The plot of the total amount of the polymer chains with the train conformation against the chain length for the same systems as in part a. The  $y$ -axis is in unit of  $a^2/6$ . In the inset, the density distributions of the train chain conformation along the  $x$ -axis at different chain lengths are displayed.

finding is that the thickness of the boundary layer is irrelevant to the degree of polymerization of the PE chains.

By exploiting the rich information of the chain configurations contained in the propagator  $q(\vec{r}, s)$ , the fractions and distributions of the different chain conformations can be obtained. The variation of the density distributions of the different chain conformations with the distance of separation between the two charged objects is studied. Figure 2a–c displays the distributions of the different chain conformations along the central horizontal line ( $x$ -axis) at different object separations for a specified set of system parameters. It can be seen from Figure 2a,b that, at a gap spacing of  $4.0R_g$ , compared to the loop fraction shown in Figure 2c, both the bridging and free chain fractions are rather low in the adsorption layer between the two charged surfaces. At such an object separation, the width of the adsorption layer in the gap between the two objects is about  $2.0R_g$  because the thickness

of the boundary layer of the adsorption chains is about  $1.0R_g$ . With the decrease in the object separation, the bridging fraction increases substantially as can be seen from Figure 2a and the inset, whereas the conformation of the free chains in the adsorption layer starts to be depleted. At a gap spacing of  $3.0R_g$ , the width of the adsorption layer between the surfaces of the two boundary layers of the respective objects is about  $1.0R_g$ , which corresponds to the coil size of the flexible PE chains, the free chains are completely depleted from the adsorption layer between the gap (see Figure 2b). Meanwhile, both the loop and the tail fractions in the adsorption layer between the two objects decrease as the two objects get closer to each other. The thickness of the boundary layers for the two charged objects in the system studied is about  $0.90R_g$  and remains unchanged when the two charged objects approach each other from a separation of  $4.50R_g$  to  $3.00R_g$ . Because the boundary layer thickness is about

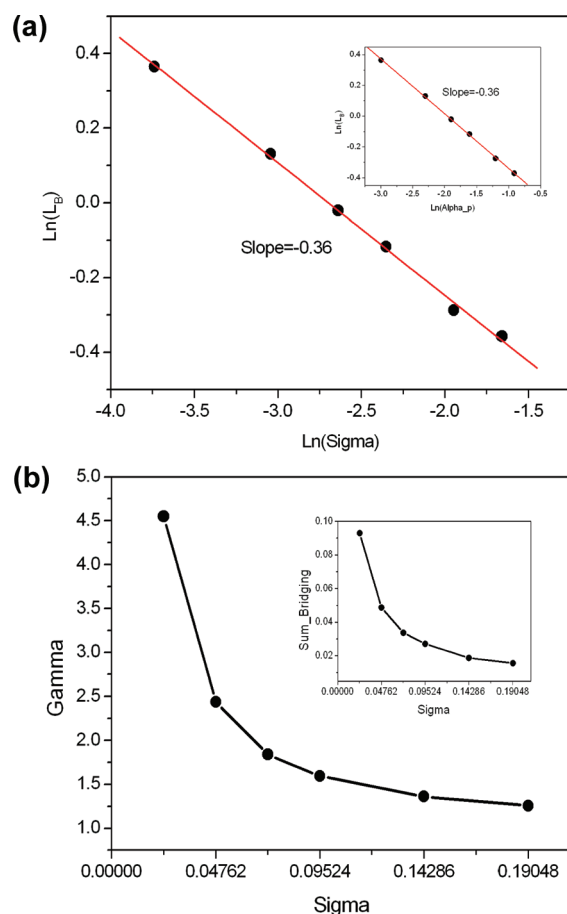


**Figure 4.** (a) Double logarithmic plot of the boundary layer thickness against the surface charge density ( $\sigma a^2 = 0.02381, 0.04762, 0.07143, 0.09524, 0.14286, 0.19048$ ) at a set of system parameters of  $N = 50$ ,  $\chi_{PS} = 0.5$ ,  $\bar{\phi}_P = 0.02$ ,  $\alpha_P = 0.2$ ,  $L_o = 2.887a$ ,  $H = 4.0R_g$ , and the system size of  $(40.0 \times 2.887a) \times (39.0 \times 2.887a)$ . There is no added salt in the system. In the inset, the double logarithmic plot of the boundary layer thickness against the charge fraction ( $\alpha_P = 0.05, 0.1, 0.15, 0.2, 0.3, 0.4$ ) at a set of system parameters of  $N = 50$ ,  $\chi_{PS} = 0.5$ ,  $\bar{\phi}_P = 0.01$ ,  $\sigma = 0.09524$ ,  $L_o = 2.887a$ ,  $H = 4.0R_g$ , and the system size of  $(40.0 \times 2.887a) \times (39.0 \times 2.887a)$  is displayed. (b) The plot of the degree of charge compensation  $\Gamma$  against the surface charge density for the same systems as in part a. In the inset, the total amount of the bridging chain conformation  $\Sigma$  is plotted against the surface charge density.

$1.0R_g$ , a single adsorption peak emerges in the gap between the two objects when the gap spacing is about  $2.0R_g$  to avoid the strong electrostatic repulsion between the two boundary layers of the two charged objects.

**2.2. Effect of the Chain Length on the Chain Conformations of the Adsorbed PE Chains.** The effect of the chain length on the chain conformations of the adsorbed PE chains is studied by varying the chain lengths while keeping all other system parameters fixed. Simulation results reveal that the boundary layer thickness is independent of the chain length, as can be seen from the inset of Figure 3a. Because the boundary layer thickness and the object separation ( $H = 3.0 \times 2.887a$ ) are the same for the cases of different chain lengths, the width of the adsorption layer between the two charged objects should be the same regardless of the chain lengths. In terms of the radius of gyration of the respective flexible chain, the width of the adsorption layer should decrease with the increase in the chain length. Therefore, the

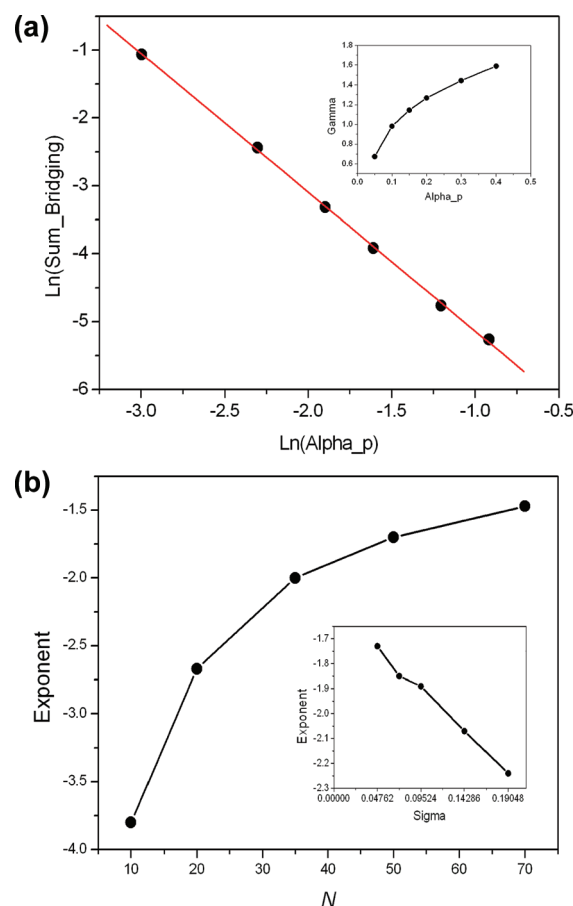


**Figure 5.** (a) Double logarithmic plot (with a slope of  $-2.04$ ) of the total amount of the bridging conformation  $\Sigma$  against the charge fraction of PE chains ( $\alpha_P = 0.05, 0.1, 0.15, 0.2, 0.3, 0.4$ ) for the same system as in the inset of Figure 4a. There is no added salt in the system. In the inset, the degree of charge compensation  $\Gamma$  is plotted against the charge fraction of PE chains. (b) The plot of the scaling exponent of the total amount of the bridging fractions with respect to the charge fraction of PE chains against the chain length at a set of system parameters of  $\chi_{PS} = 0.5$ ,  $\bar{\phi}_P = 0.02$ ,  $\sigma a^2 = 0.09524$ ,  $L_o = 2.887a$ ,  $H = 4.0R_g$ , and the system size of  $(14.0 \times 2.887a) \times (7.0 \times 2.887a)$ . There is no added salt in the system. In the inset, the scaling exponent against the surface charge density at a set of system parameters of  $\chi_{PS} = 0.5$ ,  $\bar{\phi}_P = 0.02$ ,  $N = 50$ ,  $L_o = 2.887a$ ,  $H = 4.0R_g$ , and the system size of  $(40.0 \times 2.887a) \times (39.0 \times 2.887a)$  is displayed.

bridging fraction should be the highest for the longest PE chains with  $N = 70$  and the lowest for the shortest PE chains with  $N = 10$ . This is exactly what the inset of Figure 3a shows. The effect of the chain length on the bridging chain conformation is vividly shown in the 2D contour plots of the bridging fractions in Figure 3b. As can be seen from Figure 3c, the scaling relation of the total amount of the bridging conformation  $\Sigma$  with the chain length deviates from the linear one. Nevertheless, Figure 3c suggests that the total amount of the bridging conformation follows a linear scaling law with respect to the chain length in the long polymer chain regime. The degree of chain compensation  $\Gamma$  gradually increases with the chain length, as revealed from the inset of Figure 3c.

The dependence of the train chain conformation on the chain length is also examined. It can be clearly seen from Figure 3d that, as the polymer chain length increases, the total amount of the



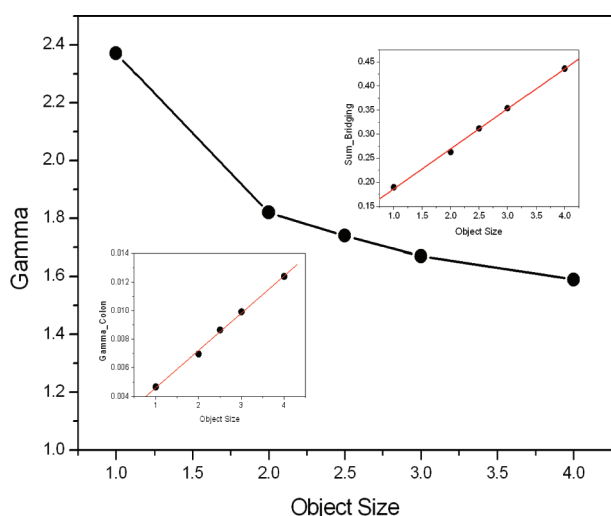


**Figure 6.** Plot of degree of charge compensation  $\Gamma$  against the size of the charged square objects ( $L_o = 2.887a, 2 \times 2.887a, 2.5 \times 2.887a, 3 \times 2.887a, 4 \times 2.887a$ ) at a set of system parameters of  $N = 50, \chi_{PS} = 0.5, \bar{\phi}_P = 0.02, \sigma a^2 = 0.04762, \alpha_P = 0.2, H = 3.0R_g$ , and the system size of  $(74.0 \times 2.887a) \times (73.0 \times 2.887a)$ . There is no added salt in the system. In the insets, the total amount of the bridging conformation  $\Sigma$  (the upper right inset) and the ratio of co-ion charges to the total surface charges (the lower left inset) are plotted against the object size, respectively.

train conformation ( $= \int_V [\phi_I^{\text{tr}}(\vec{r}) + \phi_{II}^{\text{tr}}(\vec{r})] d\vec{r}$ ) decreases and eventually approaches zero. The decrease of the total amount of the train conformation with the chain length is due to the polymer chain entropy and the independence of the boundary layer thickness of the chain length.

### 3. Dependence of the Fractions of the Different Chain Conformations on the Various System Parameters at a Fixed Object Separation and Chain Length.

**3.1. Effect of the Surface Charge Density on the Chain Conformations.** The effect of the surface charge density on the conformations of polyelectrolyte chains adsorbed on two charged objects is studied by varying the surface charge density while keeping other system parameters fixed. It is found that the thickness of the boundary layer around the two charge objects gradually decreases with increasing surface charge density. Simulation results suggest that the boundary layer thickness scales with the surface charge density as  $L_B \sim \sigma^{-0.36}$ , as shown in Figure 4a. This scaling exponent of  $-0.36$  is close to the  $-1/3$  exponent predicted in ref 14 using a scaling law argument for the adsorption of PE chains on a 1D charged surface. In deriving the  $-1/3$  exponent, the monomer–monomer electrostatic repulsion and the monomer excluded volume effect are neglected. Simulation results reveal that the degree of the charge compensation decreases with increasing surface charge density, as shown in Figure 4b. For the specific set of system parameters in Figure 4b, the total amount of charges carried by the adsorbed chains overcompensates the surface charges. The total amount of the bridging chain conformation also decreases with increasing surface charge density, as revealed from the inset of Figure 4b.

**3.2. Effect of the Charge Fraction of Polyelectrolyte Chains on the Chain Conformations.** The effect of the charge fraction of the polyelectrolyte chains with the smeared charge distribution is investigated by varying the charge fraction while keeping other system parameters fixed. Similar to the dependence of the boundary layer thickness on the surface charge density, the

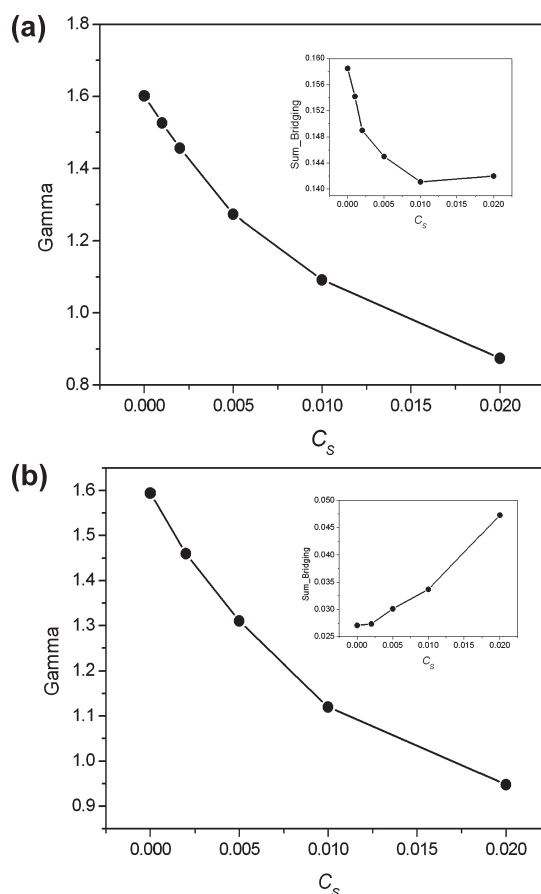


**Figure 7.** (a) Plot of the degree of charge compensation against the salt concentration ( $C_s = 0.0, 0.001, 0.002, 0.005, 0.01, 0.02$ ) at a set of system parameters of  $N = 50, \chi_{PS} = 0.5, \bar{\phi}_P = 0.02, \alpha_P = 0.2, \sigma a^2 = 0.09524, L_o = 2.887a, H = 3.0R_g$ , and the system size of  $(74.0 \times 2.887a) \times (73.0 \times 2.887a)$ . In the inset, the total amount of the bridging chain conformation is plotted against the salt concentration. (b) The plots of the degree of charge compensation against the salt concentration ( $C_s = 0.0, 0.002, 0.005, 0.01, 0.02$ ) for the same system as in part a except that  $H = 4.0R_g$  and the system size is  $(40.0 \times 2.887a) \times (39.0 \times 2.887a)$ . In the inset, the total amount of the bridging chain conformation is plotted against the salt concentration.

boundary layer thickness scales with the charge fraction of PE chains as  $L_B \sim \alpha_P^{-0.36}$  (see the inset of Figure 4a). This scaling exponent of  $-0.36$  is also close to the  $-1/3$  exponent predicted in ref 14. Simulation results reveal that the total amount of the bridging chain conformations  $\Sigma$  scales with the charge fraction of PE chains as a power law. Simulation results indicate that the scaling exponent depends on the system parameters, that is,  $N, \chi_{PS}, \bar{\phi}_P, \sigma, L_o, H$ , the salt concentration, and the system size. In Figure 5a, a typical example of the scaling relationship between the total amount of the bridging chain conformation and the charge fraction  $\alpha_P$  is displayed. The dependences of the scaling exponent on the chain length and the surface charge density at a typical set of system parameters are shown in Figure 5b. Furthermore, it is found that the degree of charge compensation  $\Gamma$  increases with the increase of the charge fraction of the PE chains (see the inset of Figure 5a).

**3.3. Effect of the Size of the Charged Objects on the Chain Conformations of the Adsorbed PE Chains.** The adsorption behaviors and chain conformations are compared for the cases of



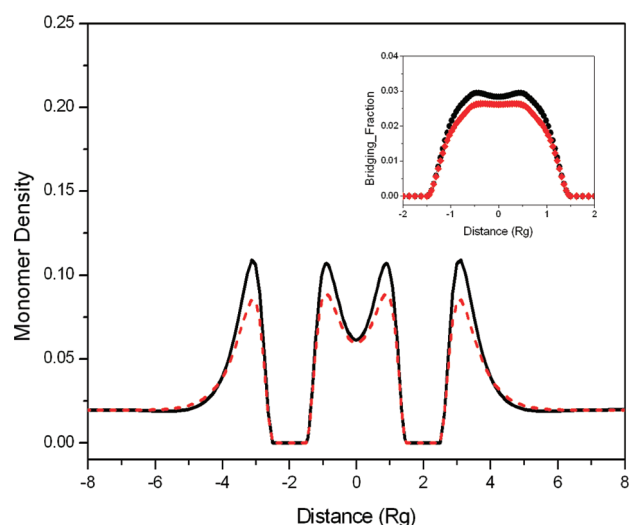


**Figure 8.** Polymer density profiles along the  $x$ -axis at different solvent qualities at a set of system parameters of  $N = 50$ ,  $\bar{\phi}_P = 0.02$ ,  $\alpha_P = 0.2$ ,  $\sigma a^2 = 0.09524$ ,  $L_o = 2.887a$ ,  $H = 3.0R_g$ , and the system size of  $(74.0 \times 2.887a) \times (73.0 \times 2.887a)$ . There is no added salt in the system. In the inset, the density distributions of the bridging conformation along the  $x$ -axis at different solvent conditions (upper curve corresponds to the  $\theta$  solvent condition) are shown. In the figure, the solid and dashed lines correspond respectively to the  $\theta$  and good solvent conditions, that is,  $\chi_{PS} = 0.5$  and  $\chi_{PS} = 0.0$ .

different sizes of the charged objects. It is found that the total amount of the bridging chain conformation  $\Sigma$  scales linearly with respect to the object size irrespective of all of the other system parameters (see the upper right inset of Figure 6). The degree of charge compensation  $\Gamma$  decreases with increasing object size, as shown in Figure 6. Interestingly, it is found that the ratio  $\Gamma_c$  of the total amount of charges of co-ions in the boundary layer to the surface charges scales linearly with respect to the object size (see the lower left inset of Figure 6). Thus, the total amount of the charges of co-ions in the boundary layer in a salt-free PE solution is quadratically proportional to the object size. It is found that the thickness of the boundary layer is nearly independent of the object size.

**3.4. Effect of the Added Salt Ions on the Chain Conformations of the Adsorbed PE Chains.** It is well-understood that the addition of salt ions to the polyelectrolyte solution will enhance the electrostatic screening effect, and at high enough salt concentrations, the PE system behaves essentially the same as a neutral polymer system. As expected, with the increase of the added salt, the total amount of the adsorbed chains quantified by  $\Gamma$  decreases, as shown in Figure 7a,b. However, the salt effect on the total amount of the bridging chain conformation  $\Sigma$  is nontrivial, as can be seen from the insets in Figure 7a,b. Compared to the total amount of the adsorbed chains, the opposite trend for the total amount of the bridging chain conformation with the increase of the salt concentration emerges in the inset of Figure 7b. The boundary layer thickness corresponding to the system in Figure 7a increases with increasing the salt concentration from  $0.90R_g$  at zero salt concentration, to  $1.00R_g$  at a salt concentration of 0.01, and to  $1.10R_g$  at a salt concentration of 0.02. Higher salt concentrations than 0.02 are not investigated because the adsorption peak and the inflection point becomes difficult to resolve due to the very weak adsorption of PE chains at such high salt concentrations.

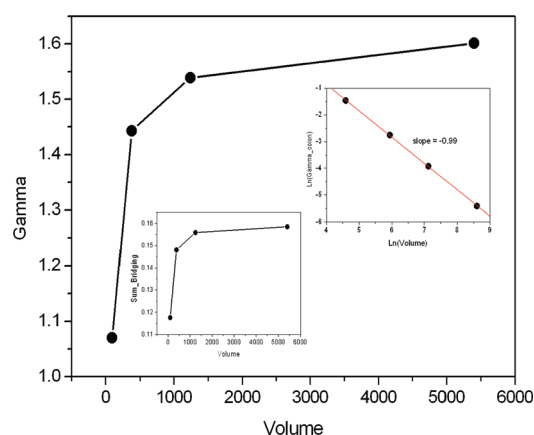


**Figure 9.** Plot of the degree of charge compensation against the volume of the system ( $14.0R_g \times 7.0R_g$ ,  $20.0R_g \times 19.0R_g$ ,  $40.0R_g \times 31.0R_g$ ,  $74.0R_g \times 73.0R_g$ ) at a set of system parameters of  $N = 50$ ,  $\bar{\phi}_P = 0.02$ ,  $\alpha_P = 0.2$ ,  $\sigma a^2 = 0.09524$ ,  $L_o = 2.887a$ , and  $H = 3.0R_g$ . There is no added salt in the system. In the lower left inset, the total amount of the bridging chain conformation is plotted against the volume of the systems. In the upper right inset, the double logarithmic plot of  $\Gamma_c$  against the volume of the system is displayed.

**3.5. Effect of the Solvent Quality on the Chain Conformations of the Adsorbed PE Chains.** We have studied the effect of the solvent quality on the chain conformations of the adsorbed chains on the charged objects. Figure 8 shows that, at the  $\theta$  solvent condition, the adsorption peaks are higher than those in the good solvent condition. This is presumably due to the stronger repulsive interaction between the monomer and the solvent molecule at the  $\theta$  solvent condition, which promotes the adsorption of PE chains on the surfaces of the charged objects. Although the adsorbed amount of PE chains on the charged objects increases in a  $\theta$  solvent, the density profiles of the different chain conformations in the adsorbed layer and the boundary layers are not affected much, as can be seen from the inset of Figure 8 (the density distributions of loop/tail conformation are not shown). The boundary layer thickness only differs slightly at the two solvent conditions and is  $0.90R_g$  and  $0.86R_g$  at the  $\theta$  solvent and the good solvent conditions, respectively.

**3.6. Effect of the Number Density of the Charged Object on the Chain Conformations of the Adsorbed PE Chains.** By varying the system size while keeping other parameters unchanged, we have studied the effect of the number density of the charged object on the adsorption behavior and the chain conformations of the PE chains. With the increase of the system size, thus with the decrease of the number density of the charged object, both the degree of charge compensation and the total amount of the bridging conformation increase dramatically at first, but eventually level off (see Figure 9 and the lower left inset). The double logarithmic plot of the ratio  $\Gamma_c$  of the total amount of charges of co-ions in the boundary layer to the surface charges against the system volume in the upper right inset of Figure 9 suggests that  $\Gamma_c$  is nearly inversely proportional to the volume of the system. This scaling relationship underscores the important entropic effect of mobile co-ions released from the charged surfaces. In the problem of the one-dimensional charged planar surface immersed in a salt-free solution, half of the total amount of ions released from the charged surfaces is confined inside the Gouy–Chapman layer. In the present study of a two-dimensional problem, the entropic effect has a profound effect on

the distribution of the co-ions released from the charged surfaces inside the boundary layer. Simulation results reveal that the boundary layer thickness is not affected by the system size.

#### IV. SUMMARY AND CONCLUSIONS

In this work, the continuum SCFT for PEs is applied to the study of the adsorption of flexible PEs onto the surfaces of two two-dimensional charged square objects with a constant electric field strength immersed in a weakly charged polyelectrolyte solution. Both the modified diffusion equation describing the chain conformations and the Poisson equation for the electrostatics within the set of SCFT equations are solved by the efficient multigrid method. Two-dimensional Cartesian grids are used with the two charged objects excluded from the computational domain.

The effective interaction between the two charged objects is examined. At specific sets of system parameters, the emergence of an attractive interaction between the two charged objects mediated by the PE chains is observed. It is found that the impact of the bridging effect of PE chains between the two charged objects on the free energy of one polyelectrolyte chain stems from the entropic effects of polymer chains, counterions, and co-ions.

Simulation results show that the thickness of the boundary layer is independent of the chain length, having dependences on the surface charge density, the fraction of charges on the PE chains, and the salt concentration. Simulation results suggest that the boundary layer thickness scales with the surface charge density and the fraction of charges on the PE chains as  $L_B \sim \sigma^{-0.36}$  and  $L_B \sim \alpha_P^{-0.36}$ , respectively. We have introduced the parameter of the degree of charge compensation to quantify the total amount of charges on the adsorbed PE chains in the system. It is found that the total amount of the charges on the adsorbed chains can overcompensate the opposite charges on the two objects for relatively long PE chains with high charge fractions.

The dependences of the fractions of tail, loop, train, and bridge conformations on different controlling parameters are investigated by solving the modified diffusion equation with appropriate boundary conditions on the surfaces of the boundary layers and the two charged objects. First, the dependence of the different chain conformations on the separation between the two charged objects is studied. Simulation results reveal that, when the width of the adsorption layer between the two charged objects is reduced to about  $2.0R_g$ , the bridging fraction starts to increase substantially. As the two charged objects get further closer, with the increase in the bridging fraction, the loop/tail fractions gradually decrease, and the free chain conformation is depleted in the adsorption layer between the two objects. When the separation between the two charged objects is small enough such that the two boundary layers would begin to overlap, a single adsorption layer between the two charged objects emerges instead. The effect of the chain length on the chain conformations at a fixed object separation is studied. Consistent with experimental observations, an increase in the polyelectrolyte chain length results in the increase in the bridging fraction in the gap between the two charged objects. Simulation results suggest that the total amount of the bridging chain conformation in the system scales linearly with respect to the chain length in the long polymer chain regime.

The dependences of the different chain conformations on various system parameters at a fixed object separation and chain

length are studied. It is found that the loop and tail fractions in the adsorption layer between the two charged objects always follow the same trend with respect to any of the system parameters studied. Simulation results reveal that the total amount of the bridging chain conformations in the system scales with the charge fraction of PE chains as a power law. Investigations further suggest that the scaling exponent depends on all of the other system parameters. It is also found that the total amount of the bridging chain conformation in the system scales linearly with the size of the charged objects.

Finally, we discuss the limitations of the present model and the approximations used in this work. Because the SCFT is a mean-field theory with the Gaussian chain model embedded in, it only applies to weakly charged and flexible polyelectrolyte solutions where the effect of the charge correlation can be neglected. For the study of strongly charged polyelectrolyte systems, molecular simulations are generally required. In this work, for simplicity, the spatial distribution of the electric permittivity due to the large difference between the hydrophobic monomers and polar water molecules is not taken into account. The short-range non-Coulombic interaction between the surfaces of the charged objects and the PE chains is not considered. For numerical convenience, square objects instead of the spherical or circular ones are used to study the adsorption of PE chains. Another approximation is that the mobile ions are assumed to be point-like charges. Work along these lines to study the more realistic problem of the polyelectrolyte adsorption on charged surfaces is ongoing and will be the subject of future publications.

#### AUTHOR INFORMATION

##### Corresponding Author

\*E-mail: tongchaohui@nbn.edu.cn or ctong0@hotmail.com.

#### ACKNOWLEDGMENT

The authors thank the financial support from the National Natural Science Foundation of China (NSFC projects 21074062, 20990230, 11174163, 20874019) and the Scientific Research Foundation for the Returned Overseas Chinese Scholars, State Education Ministry. C.T. acknowledges the supports from K. C. Wong Magna and Hu Lan Funds at Ningbo University.

#### REFERENCES

- (1) Dautzenberg, H.; Jaeger, W.; Kotz, J.; Philipp, B.; Seidel, C.; Stscherbina, D. *Polyelectrolytes: Formation, Characterization and Application*; Hanser Gardner: Munich, Germany, 1994.
- (2) Fleer, G. J.; Cohen Stuart, M. A.; Scheutjens, J. M. H. M.; Gaskove, T.; Vincent, B. *Polymer at Interfaces*; Chapman and Hall: London, 1993.
- (3) Kawaguchi, M.; Takahashi, A. *Adv. Colloid Interface Sci.* **1992**, *37*, 219–317.
- (4) Naji, A.; Seidel, C.; Netz, R. R. *Adv. Polym. Sci.* **2006**, *198*, 149–183.
- (5) Claesson, P. M.; Dedinaite, A.; Rojas, O. J. *Adv. Colloid Interface Sci.* **2003**, *104*, 53–74.
- (6) Dobrynin, A. V. *Curr. Opin. Colloid Interface Sci.* **2008**, *13*, 376–388.
- (7) Podgornik, R.; Licer, M. *Curr. Opin. Colloid Interface Sci.* **2006**, *11*, 273–279.
- (8) Boroudjerdi, H.; Kim, Y. W.; Naji, A.; Netz, R. R.; Schlagberger, X.; Serr, A. *Phys. Rep.* **2005**, *416*, 129–199.
- (9) Netz, R. R.; Andelman, D. *Phys. Rep.* **2003**, *380*, 1–95.

- (10) Naji, A.; Jungblut, S.; Moreira, A. G.; Netz, R. R. *Physica A* **2005**, 352, 131–170.
- (11) Claesson, P. M.; Poptoshev, E.; Bloomberg, E.; Dedinaite, A. *Adv. Colloid Interface Sci.* **2005**, 114, 173–187.
- (12) Muthukumar, M. J. *Chem. Phys.* **1987**, 86, 7230–7235.
- (13) Feng, X. H.; Dubin, P. L.; Zhang, H. W.; Kirtan, G. F.; Bahadur, P.; Parotte, J. *Macromolecules* **2001**, 34, 6373–6379.
- (14) Shafir, A.; Andelman, D.; Netz, R. R. *J. Chem. Phys.* **2003**, 119, 2355–2362.
- (15) (a) Winkler, R. G.; Cherstvy, A. G. *Phys. Rev. Lett.* **2006**, 96, 066103. (b) Cherstvy, A. G.; Winkler, R. G. *J. Chem. Phys.* **2004**, 120, 9394–9340. (c) Cherstvy, A. G.; Winkler, R. G. *J. Chem. Phys.* **2006**, 125, 064904. (d) Winkler, R. G.; Cherstvy, A. G. *J. Phys. Chem. B* **2007**, 111, 8486–8493.
- (16) Wallin, T.; Linse, P. *J. Phys. Chem. B* **1997**, 101, 5506–5513.
- (17) Netz, R. R.; Joanny, J. F. *Macromolecules* **1999**, 32, 9013–9025.
- (18) Yang, S.; Yan, D. D.; Shi, A. C. *Macromolecules* **2006**, 39, 4168–4174.
- (19) Licer, M.; Podgornik, R. *J. Phys.: Condens. Matter* **2010**, 22, 414102.
- (20) Podgornik, R. *J. Chem. Phys.* **2003**, 118, 11286–11296.
- (21) Goeler, F. V.; Muthukumar, M. J. *Chem. Phys.* **1994**, 100, 7796–7803.
- (22) Borukhov, I.; Andelman, D.; Orland, H. *J. Phys. Chem. B* **1999**, 103, 5042–5057.
- (23) Huang, H.; Ruckenstein, E. *Adv. Colloid Interface Sci.* **2004**, 112, 37–47.
- (24) Huang, H.; Ruckenstein, E. *Langmuir* **2006**, 22, 3174–3179.
- (25) Turesson, M.; Forsman, J.; Akesson, T. *Langmuir* **2006**, 22, 5734–5741.
- (26) Turesson, M.; Akesson, T.; Forsman, J. *Langmuir* **2007**, 23, 9555–9558.
- (27) Luckham, P. F.; Klein, J. J. *Chem. Soc., Faraday Trans.* **1984**, 1, 865–878.
- (28) Abraham, T.; Kumpulainen, A.; Xu, Z.; Rutland, M.; Claesson, P. M.; Masliyah, J. *Langmuir* **2001**, 17, 8321–8327.
- (29) Goubault, C.; Leal-Caldron, F.; Viovy, J. L.; Bibette, J. *Langmuir* **2005**, 21, 3725–3729.
- (30) Arya, G. J. *Phys. Chem. B* **2009**, 113, 15760–15770.
- (31) Arya, G. J. *Phys. Chem. B* **2010**, 114, 15886–15896.
- (32) Hu, Y. Y.; Ni, R.; Cao, D. P.; Wang, W. C. *Langmuir* **2008**, 24, 10138–10144.
- (33) Hu, Y. Y.; Cao, D. P. *Langmuir* **2009**, 25, 4965–4972.
- (34) (a) Tian, W. D.; Ma, Y. Q. *Macromolecules* **2010**, 43, 1575–1582. (b) Ren, C. L.; Tian, W. D.; Szleifer, I.; Ma, Y. Q. *Macromolecules* **2011**, 44, 1719–1727.
- (35) Daoulas, K. C.; Theodorou, D. N.; Harmandaris, V. A.; Karayiannis, N. C.; Mavrantzas, V. G. *Macromolecules* **2005**, 38, 7134–7149.
- (36) Semenov, A. N.; Bonet-Avalos, J.; Johnner, B. A.; Joanny, J. F. *Macromolecules* **1996**, 29, 2179–2196.
- (37) Scheutjens, J. M. H. M.; Fleer, G. J. *J. Phys. Chem.* **1979**, 83, 1619–1635.
- (38) Scheutjens, J. M. H. M.; Fleer, G. J. *J. Phys. Chem.* **1980**, 84, 178–190.
- (39) Scheutjens, J. M. H. M.; Fleer, G. J. *Macromolecules* **1985**, 18, 1882–1900.
- (40) Van der Schee, H. A.; Lyklema, J. *J. Phys. Chem.* **1984**, 88, 6661–6667.
- (41) Shi, A. C.; Noolandi, J. *Macromol. Theory Simul.* **1999**, 8, 214–229.
- (42) Wang, Q.; Taniguchi, T.; Fredrickson, G. H. *J. Phys. Chem. B* **2004**, 108, 6733–6744.
- (43) Wang, Q. *Macromolecules* **2005**, 38, 8911–8922.
- (44) Wang, Q. *J. Phys. Chem. B* **2006**, 110, 5825–5828.
- (45) Man, X.; Yang, S.; Yan, D. D.; Shi, A. C. *Macromolecules* **2008**, 41, 5451–5456.
- (46) (a) Witte, K. N.; Won, Y. Y. *Macromolecules* **2006**, 39, 7757–7768. (b) Witte, K. N.; Won, Y. Y. *Macromolecules* **2008**, 41, 2735–2738.
- (47) Yang, S.; Vishnyakov, A.; Neimark, A. V. *J. Chem. Phys.* **2011**, 134, 054104.
- (48) Press, W. H.; Teukolsky, S. A.; Vetterling, W. T.; Flannery, B. P. *Numerical Recipe in Fortran 77: the Art of Scientific Computing*, 2nd ed.; Cambridge University Press: New York, 1999; Chapter 19.6.
- (49) (a) Tong, C.; Wu, T.; Provatas, N. *Model. Simul. Mater. Sci. Eng.* **2006**, 14, 1447–1464. (b) Pan, Q. Y.; Tong, C. H.; Zhu, Y. J. *ACS Nano* **2011**, 5, 123–128.
- (50) Quarteroni, A.; Valli, A. *Domain Decomposition Methods for Partial Differential Equations*; Oxford University Press: Oxford, U.K., 1999.